THE JOURNAL OF PHYSICAL CHEMISTRY C

Article

pubs.acs.org/JPCC

Effect of Anchoring Groups on Single Molecule Charge Transport through Porphyrins

Zhihai Li,[†] Manuel Smeu,[‡] Mark A. Ratner,*[,‡] and Eric Borguet*[,†]

[†]Department of Chemistry, Temple University, Philadelphia, Pennsylvania 19122, United States

[‡]Department of Chemistry, Northwestern University, Evanston, Illinois 60208, United States

Supporting Information

ABSTRACT: Controlling charge transport through individual molecules and further understanding the effect of anchoring groups on charge transport are central themes in molecule-based devices. However, in most anchoring effect studies, only two, or at most three nonthiol anchoring groups were studied and compared for a specific system, i.e., using the same core structure. The scarcity of direct comparison data makes it difficult to draw unambiguous conclusions on the anchoring group effect. In this contribution, we focus on the single molecule conductance of porphyrins terminated with a range of anchoring groups: sulfonate ($-SO_3^-$), hydroxyl ($-OH$), nitrile ($-CN$), amine ($-NH_2$), carboxylic acid ($-COOH$), benzyl ($-C_6H_6$), and pyridyl ($-C_6H_5N$). The present study represents a first attempt to investigate a broad series of anchoring groups in one specific molecule for a direct comparison. It also is the first attempt, to our knowledge, to explore single molecule conductivity with two novel anchoring groups sulfonate ($-SO_3^-$) and hydroxyl ($-OH$). Our experimental results reveal that the single molecule conductance values of the porphyrins follow the sequence of pyridyl > amine > sulfonate > nitrile > carboxylic acid. Electron transport calculations are in agreement that the pyridyl groups result in higher conductance values than the other groups, which is due to a stronger binding interaction of this group to the Au electrodes. The finding of a general trend in the effect of anchoring groups and the exploration of new anchoring groups reported in this paper may provide useful information for molecule-based devices, functional porphyrin design, and electron transfer/transport studies.

INTRODUCTION

Nanoscale devices incorporating individual molecules have been achieved in some systems[1,2] using tailored molecules as functional electrical components to perform certain operations, e.g., transistors,[3] amplifiers,[4] and switches.[5] Measuring and understanding the electrical characteristics of single-molecule conductance (SMC) in molecular electronics is as important as determining the electrical properties (conductance/resistance, switching, gating) of macro devices in conventional electronics.[6,7] One effective approach to measuring the conductance of single molecules is the scanning tunneling microscopy (STM) break junction technique[8] initially demonstrated by Tao[9] and developed by other groups.[10−15] In this method, functional (anchoring) groups were introduced to behave as "alligator clips" connecting a molecule to two electrodes (an STM tip and a substrate), making it possible to measure single molecule/junction conductance.[16] In the simplest qualitative analysis, the conductance of a single molecule in a nanoscale junction is determined by both the resistance of the molecular core (R2, Figure 1B) and the contact resistance (R1, Figure 1B). Thus, understanding the effect of anchoring groups on electron transport through individual molecules is paramount to fabricating molecular devices as well as the accurate measurement and understanding of the electrical conductance of molecules—the basic building blocks in molecular electronics.

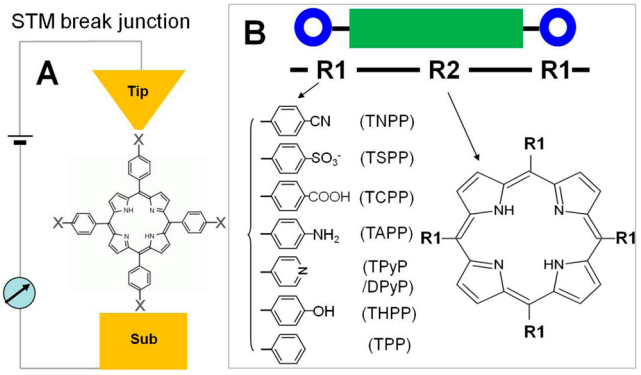

Figure 1. (A) Schematic of a porphyrin connected to two electrodes in an STM break junction with different anchoring groups; (B) illustration of a porphyrin (R2) terminated with one of the seven distinct groups (R1) investigated in this study. The local resistances (R1, R2) are for heuristic purposes.

Received: October 5, 2012
Revised: June 20, 2013
Published: July 11, 2013

dx.doi.org/10.1021/jp309871d | J. Phys. Chem. C 2013, 117, 14890−14898

The effect of anchoring groups on single molecule conductance (SMC) has been explored by using different molecular systems[16−18] and anchoring groups, including thiol,[3,19] carbothioate (−CS_2H),[14,20] isocyanide (−NC),[10,16,18] nitrile (−CN),[21−23] amine (−NH_2),[11,15,17] pyridine,[24] fullerene,[25,26] carboxylic acid (−COOH),[17] selenium (−Se),[27] tellurium (−Te),[27] nitro (−NO_2),[22] and isothiocyanate (−NCS).[28] However, these groups have been investigated most frequently when connected to nonhighly conjugated molecular cores, e.g., saturated alkanes,[15,17,29] that are expected to have poor intrinsic conductivity, rather than in highly conjugated systems[30] that are more probable candidates for molecular wires, though there are a few reports of comparison of anchoring groups in conjugated systems.[16,22,23] In saturated systems, the resistance from the core structure (R2, Figure 1B) is higher and, as a consequence, the anchoring effect is diminished. Furthermore, in most existing anchoring effect studies, only one, two,[15,16,18] or at most three nonthiol[17,22,23] anchoring groups were studied and compared for a specific system, i.e., using the same core structure. Thus, our current understanding of the effect of anchors is mainly from results using different molecular cores under different experimental conditions and/or measuring techniques. This can be considered an "indirect" comparison. A direct comparison would require measurements of a range of anchoring groups on the same molecular core with a single technique. The scarcity of direct comparison data makes it difficult to draw unambiguous conclusions on the anchoring group effects.

As a unique class of compounds, porphyrins play an important role in biological processes (transport of oxygen, biocatalysis, etc.). The study of electron transport through porphyrins is fundamentally important to many fields, e.g., biological engineering and sensors. Nevertheless, only a few studies on SMC of porphyrin derivatives[31−33] or wires[34,35] have been reported and the detailed understanding of electron transport through porphyrins is still insufficient. Except for two reports by Nichols et al., employing pyridyl anchoring groups,[34,36,37] all other studies have focused on the SMC measurement of thiolated porphyrin derivatives,[31,32,35,38] and there is no report, to the best of our knowledge, of the anchoring effect on the SMC of porphyrins.

In this paper, we choose porphyrins as a backbone/core structure and focus on the SMC of porphyrins terminated with a range of nonthiol anchoring groups: sulfonate (−SO_3^-), hydroxyl (−OH), nitrile (−CN), amine (−NH_2), carboxylic acid (−COOH), benzyl (−C_6H_6), and pyridyl (−C_6H_5N), named TSPP, THPP, TNPP, TAPP, TCPP, TPP, and TPyP, respectively (Figure 1, Figure S1). Our results reveal that the SMC of porphyrins follows the sequence of pyridyl > amine > sulfonate > nitrile > carboxylic acid. Calculations show that electron-donating and electron-withdrawing groups can change the energy of the LUMO and HOMO. However, the HOMO−LUMO gaps (for the porphyrins studied here) are almost the same. Possible correlations between SMC and a number of different parameters such as binding strength, electron-donating/withdrawing effect, electron density, energy band gap between the highest occupied molecular orbital (HOMO) and lowest unoccupied molecular orbital (LUMO), etc. are discussed.

EXPERIMENTAL SECTION

1. Chemicals. 5,10,15,20-Tetraphenyl-21*H*,23*H*-porphine (TPP, >99%) was obtained from Sigma-Aldrich; 5,10,15,20-tetra(4-pyridyl)-21*H*,23*H*-porphine (TPyP, synthetic, 97%) was obtained from Aldrich. Tetra(4-carboxyphenyl)porphine (TCPP), tetra(4-cyanophenyl)porphine (nitrile side groups, TNPP); tetra(4-aminophenyl)porphine (TAPP), 5,15-di(4-pyridyl)-10,20-diphenylporphyrin (p-DPyP), 5,10-di(4-pyridyl)-15,20-diphenylporphyrin (o-DPyP), tetra(4-sulfonatophenyl)porphine (TSPP), and tetrahydroxyphenylporphine (THPP) were obtained from Frontier Scientific (synthetic, >95%). Chloroform (anhydrous, >99%), tetrahydrofuran (THF, anhydrous, >99.9%, inhibitor free), and mesitylene (1,3,5-trimeththylbenzene, puriss, >99.0%) were obtained from Sigma-Aldrich. Ethanol (absolute, anhydrous, ACS/USP grade) was obtained from Pharmco-Aaper.

2. Modification of Electrode with Molecules. The Au(111) substrate electrode for break junction experiments was a single crystal disc (10 mm diameter, 2.0 mm thick) purchased from MaTeck, Germany. Gold wire (0.25 mm in diameter, premion, 99.999%) was purchased from Alfa Aesar. STM tip electrodes were prepared by mechanically cutting a gold wire.

Before each experiment, single crystal substrates were annealed for 2 min in a hydrogen flame at red heat, followed by quenching in ultrapure (Milli-Q) water saturated with hydrogen and then dried with a stream of high purity argon. Molecular modification of the electrodes took place by immersing the dry gold crystal in 0.05 mM chloroform or tetrahydrofuran (TCPP, TNPP, THPP) or ethanol (TSPP) solution containing target molecules for 1 min at room temperature followed by rinsing with the pure solvent 3 times.

3. STM Break Junction Experiments. The STM break junction experiments were carried out with a Molecular Imaging Picoscan or Picoplus microscope (Agilent), using Picoscan 5.3.3 software. We first cleaned a Teflon liquid cell and Teflon O-ring with Piranha solution and rinsed the cell and O-ring with the ultrapure water and dried them first with argon and then in an oven at 110 °C for 30 min. Then, the cell and O-ring were assembled onto the molecule-modified electrode and mesitylene solvent was added to the STM cell.

Parameters were set up to allow the STM program to drive the tip to approach the molecule-modified electrode, typically at a bias voltage (V_{bias}) of 0.2 V and tunneling set point (i_T) of 0.1 nA. After the STM tip was engaged, the electrode surface was first imaged by STM in constant current mode confirming a clean surface and a sharp tip with typical parameters: i_T = 0.1 nA, V_{bias} = 0.1 V; scan size = 200 nm × 200 nm, scan speed = 200−500 nm/s. The *z*-direction drift of the tip was checked by switching off the STM feedback loop and simultaneously monitoring the tunneling current versus time. When the tunneling current changes by less that 20% in 10 s, we regard the drift as substantially reduced. At that point the tip was positioned on a large terrace (about 100 nm wide or more). Then the STM feedback loop was switched off and the tip was driven into contact with the substrate to form a junction at a sweep rate of 10−20 nm/s. The tip was then retracted to break the contact. During the retracting process, the current versus distance traces were recorded. The process of forming and breaking of junctions was repeated many times and a large number of current−distance traces were recorded, typically 5000 traces in our experiments for statistical analysis.

4. Single Molecule Conductance Measurement. We deposited the target molecules on the gold substrate electrode and drive another electrode (a gold STM tip) toward the substrate electrode to form an electrode−electrode contact. Then the STM tip was retracted from the substrate electrode to

dx.doi.org/10.1021/jp309871d | J. Phys. Chem. C 2013, 117, 14890−14898

form metal nanojunctions. Extension of the metal nanojunction results in quantized current steps (1 G_o, 2 G_o, etc.) in the current−distance traces.[9] Further retraction of the tip electrode results in the breaking of the metal contact junction. If there is no molecule bridging the two electrodes after the metal junction/wire breaks, one observes current traces that exponentially decay with retraction distance[9] (Figure 2A, gray). However, if a molecule bridges the gap between the two electrodes, a molecular junction is formed, revealed as a current plateau or step (Figure 2A black and colored traces) in the current−distance trace.[9]

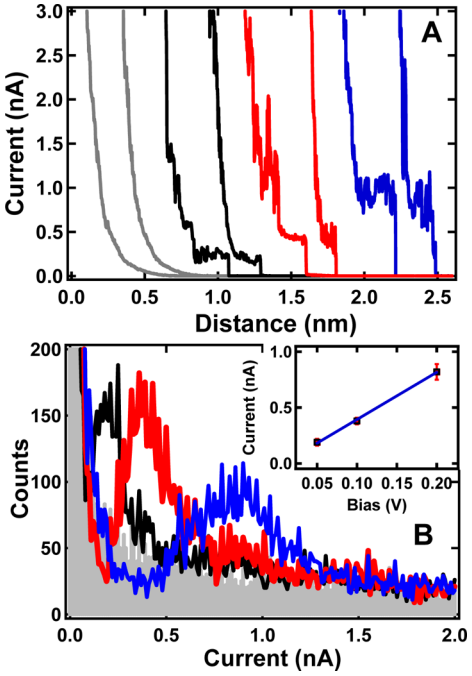

Figure 2. (A) Examples of individual current−distance traces measured during STM break junction experiments for tetra(cyano/nitrile)porphine (TNPP) at V_{bias} = 0.05 (black), 0.1 (red), and 0.2 V (blue). The gray curves represent traces without molecular junction formation at 0.1 V; (B) current histograms constructed from stepped current−distance traces measured at V_{bias} = 0.05 (black), 0.1 (red), and 0.2 V (blue), respectively. The gray background is built from the traces without molecular junction formation. Inset: Current maximum from the histogram in part B as a function of bias voltage. The solid line is a straight line fit.

Several sample-stepped current−distance traces for TNPP (Figure 2A) were measured at three biases (0.05, 0.1, and 0.2 V) with a tip displacement rate of 12 nm/s. The traces show that the step/plateau currents increase with the bias voltage applied. All the stepped traces were used to construct the current histograms to determine the molecular conductance. The stepped traces were selected based on the criteria that they should contain at least one step longer than 0.05 nm. In contrast to the gray curve in Figure 2A, constructed from current−distance traces without steps, the black curve constructed by 102 traces out of the total 1000 traces shows a current maximum around 0.19 ± 0.03 nA at a bias voltage of 0.05 V (Figure 2B). The red and blue curves (Figure 2B) were constructed from individual traces measured at biases of 0.1 (Figure 2A, red) and 0.2 V (Figure 2A, blue), and show the current peaks of 0.38 ± 0.03 and 0.82 ± 0.07 nA, respectively. The slope of the linear fit of the current vs bias voltage indicates the molecular conductance of 4.11 ± 0.48 nS (5.3×10^{-5} G_o, where G_o = 77 500 nS) (Figure 2).

COMPUTATIONAL DETAILS

1. Electronic Structure of Isolated Molecules. Density functional theory (DFT) calculations on isolated molecules were carried out with the GAMESS electronic structure package.[39] The approach used was to relax the geometry of the molecules and to calculate the energies of their highest occupied and lowest unoccupied molecular orbitals (HOMO/LUMO). The B3LYP hybrid functional[40,41] was used with the 6-31G(d) basis set.

2. Periodic Calculations of Molecule on Au Surface and Two-Probe Relaxations. Periodic boundary calculations were used to relax larger structures for calculating the binding energy of the system shown in Figure 3A and the central region for the two-probe transport structures shown in Figure 3B. These calculations were carried out with the Vienna ab initio simulation package (VASP),[42,43] using the Perdew−Burke−Ernzerhof generalized gradient approximation (PBE-GGA).[44] A projector augmented wave method was used for the ionic potentials,[45,46] with a kinetic energy cutoff for the plane wave basis of 400 eV.

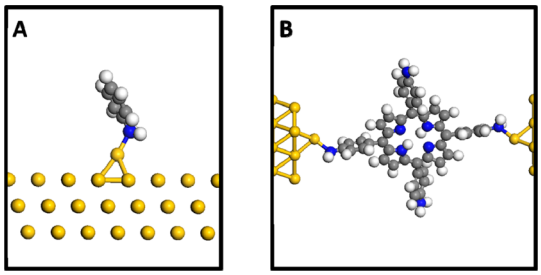

Figure 3. (A) Benzene with amine group interacting with Au adatom on top of the Au(111) surface in a periodic supercell. (B) Periodic structure used to relax the molecule between two Au electrodes.

During the structure relaxations for the binding energy (Figure 3A), all Au atoms in the surface were frozen to their bulk positions while the Au adatom sitting on top and all other atoms were allowed to relax until the net force was less than 0.01 eV/Å. The extended porphyrin molecule was truncated to contain just the phenyl group immediately connected to the anchoring group in order to save on computational cost. We expect the general trend in binding energies for the different anchoring groups not to be significantly affected by this smaller model. For the two-probe structure relaxations (see Figure 3B), all Au atoms were frozen to bulk positions with the exception of the Au adatoms interacting with each end of the molecule. All other atoms were allowed to relax until the net force was less than 0.02 eV/Å. This procedure was repeated for various electrode−electrode separations to find the minimum-energy structure for each molecule. For all VASP calculations, sufficient vacuum was included in the supercell so that the molecule would not interact with its image in neighboring cells. Note that even though these were periodic calculations, only the Gamma point of the Brillouin zone was sampled since these supercells are larger than 10 Å in each direction.

3. Electron Transport Calculations. The electron transport calculations are performed on a two-probe geometry, as the one shown in Figure 4. In this system, the left and right electrodes are semi-infinite, repeating to the left and right,

dx.doi.org/10.1021/jp309871d | J. Phys. Chem. C 2013, 117, 14890−14898

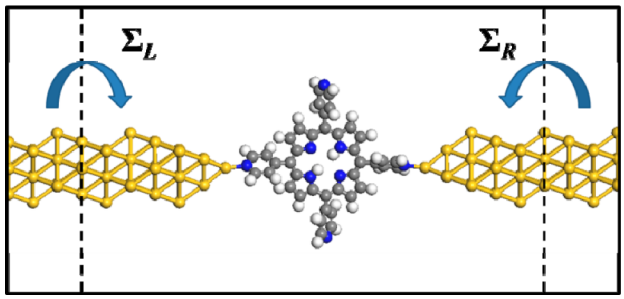

Figure 4. Two-probe transport structure. The left and right electrodes are repeated to infinity. The effect of the electrodes on the central (molecular) region is included in the self-energies, $\Sigma_{L/R}$.

respectively. The central region contains the molecule of interest as well as a portion of each electrode. The effects of the left/right electrodes on the central region are included as self-energy terms $\Sigma_{L/R}$, as described below.

We used a quantum transport computation technique that employs density functional theory (DFT) within the non-equilibrium Green's function (NEGF) formalism as implemented in the Nanodcal electron transport code.[47] This approach has been extensively described in the literature (for example, see refs 48 and 49), hence only a basic summary is provided here. The NEGF-DFT technique is an iterative procedure in which the Hamiltonian and the electronic structure of the two-probe transport structure are calculated by DFT in a conventional manner, but the levels are populated based on nonequilibrium statistics obtained from the NEGF. During this procedure, the retarded Green's function at energy E is obtained by inverting the Hamiltonian matrix, $G(E) = [(E + i\eta)S - H - \Sigma_L - \Sigma_R]^{-1}$, where H and S are the Hamiltonian and overlap matrices for the central region determined with DFT. η is a positive infinitesimal and $\Sigma_{L/R}$ are self-energies that account for the effect of the left and right electrodes on the molecular region. The self-energy is a complex quantity with its real part representing a shift of the energy levels and its imaginary part representing their broadening, which can be expressed as the broadening matrix, $\Gamma_{L,R} = i(\Sigma_{L,R} - \Sigma_{L,R}^{\dagger})$. The self-energy is calculated within the NEGF-DFT formalism by an iterative technique.[50] From these quantities, the electronic density matrix can be obtained as, $\rho = (1/2\pi)\int_{-\infty}^{\infty}[f(E,\mu_L) G\Gamma_L G^{\dagger} + f(E,\mu_R) G\Gamma_R G^{\dagger}]\, dE$, where $\mu_{L,R}$ are the electrochemical potentials of the left and right electrodes and $f(E,\mu)$ is the Fermi–Dirac function that describes the population for a given energy and electrochemical potential. The density obtained from the above equation is used in a subsequent DFT iteration step and the cycle is repeated until self-consistency is achieved. The transmission function is then obtained from the Green's function as $T(E) = \mathrm{Tr}(\Gamma_L G \Gamma_R G^{\dagger})$, which represents the probability that an electron with a given energy E transmits from one electrode, through the molecular region, into the other electrode. The transmission near the Fermi energy[51] of the electrodes is related to the low-bias conductance of the molecule.

In the NEGF-DFT calculations, norm-conserving pseudopotentials[52] were used to describe the atomic cores and double-ζ polarized (DZP) numerical orbitals for the valence electrons, and the exchange-correlation was treated using the GGA-PBE functional.[50]

RESULTS AND DISCUSSION

The SMC measurements (Experimental Section) were performed for porphyrins with different nonthiol anchoring groups, i.e., sulfonate (TSPP), hydroxyl (THPP), nitrile (−CN), carboxylic acid (TCPP), amine (TAPP), and pyridyl (TPyP). Note that neither sulfonate nor hydroxyl, to the best of our knowledge, have been employed in SMC as anchoring groups though they are popular functional groups in organic chemistry. This motivates us to investigate the possibility of using these groups as anchoring units in break junction measurements. Our experiments show that the sulfonate group can work as an anchor in STM break junctions (Figure 5).

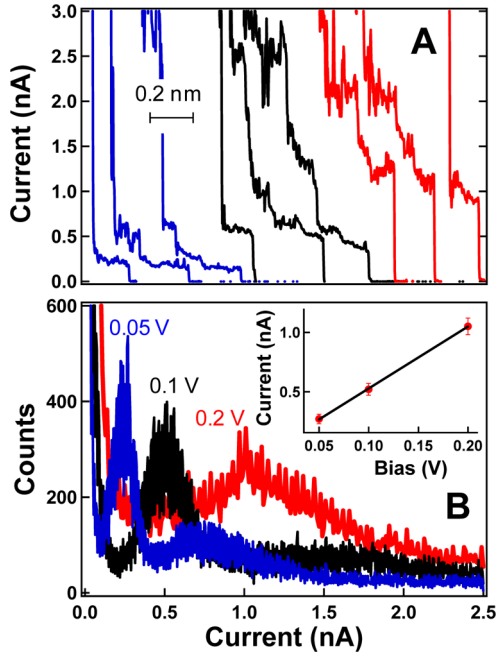

Figure 5. (A) Example individual current–distance traces for tetra(4-sulfonatophenyl)porphine (TSPP) measured at three biases: 0.05 (blue), 0.1 (black), and 0.2 V (red). (B) Current histograms constructed for biases of 0.05, 0.1, and 0.2 V, respectively. Inset: Current maxima from the histogram in part B as a function of bias voltage. The solid line is a straight line fit.

Individual current–distance traces (Figure 5A) measured at different bias voltages (0.05, 0.10, and 0.20 V) display current step-like features corresponding to the formation of molecular junctions between the STM tip and the substrate.[9] The traces show that the step/plateau currents increase with the applied bias voltage. All the stepped traces were used to construct the current histograms to determine the molecular conductance. The stepped traces are 10–30% of the total recorded traces in our experiments. The rest, exponentially decaying traces and occasionally observed noisy traces (less than 5%), were rejected because these curves contribute a large background peak near zero current.[14,17,53] (see the Experimental Section). The current histograms in Figure 5B were constructed by using 263 (blue), 396 (black), and 409 (red) stepped traces from each 2000 total traces showing current maxima at around 0.27, 0.52, and 1.05 nA, respectively. The molecular conductance (5.2 nS) can be determined from the linear fit of current vs bias plotting (Figure 5B, inset). The error bars (Table 1 and Figure 5) are based on the standard deviation of the most probable conductance (peak of histogram) measured in multiple

dx.doi.org/10.1021/jp309871d | J. Phys. Chem. C 2013, 117, 14890–14898

Table 1. Summary of Single Molecule Conductance of Porphyrins Measured in STM Break Junction Experiments and Several Other Quantities Obtained from Calculations[a]

anchoring group	SMC (nS)	SMC (G_o)	end-to-end length (nm)	binding energy (eV)	HOMO (eV)	LUMO (eV)	HOMO−LUMO gap (eV)	trans. peak height
o-DPyP	28.0 ± 2.4	3.6×10^{-4}	1.10	−1.1	−5.09	−2.38	2.71	0.98
TPyP	20.5 ± 3.5	2.65×10^{-4}	1.56	−1.1	−5.38	−2.65	2.73	0.99
p-DPyP	19.7 ± 2.1	2.5×10^{-4}	1.56	−1.1	−5.09	−2.40	2.69	0.99
TAPP	5.91 ± 0.40	7.6×10^{-5}	1.84	−0.8	−4.39	−1.77	2.61	0.71
TSPP	5.2 ± 0.4	6.7×10^{-5}	2.01	−0.3	−5.63	−2.89	2.74	*b*
TNPP	4.11 ± 0.48	5.3×10^{-5}	2.08	−0.9	−5.65	−2.93	2.71	0.53
TCPP	2.67 ± 0.26	3.5×10^{-5}	1.98	−0.6	−5.22	−2.54	2.68	0.98

[a]The molecular orbital energies were obtained from calculations on isolated molecules. [b]See ref56.

different experiments performed on different days. In addition, there is a shallow broad peak at a higher current range (Figure 5B, blue) that could be due to the presence of multiple molecules in a junction.[9,17]

The break junction experiment was performed in the same way for porphyrins having nitrile (−CN, TNPP), carboxylic acid (−COOH, TCPP), and amine ($-NH_2$, TAPP) anchoring groups. The SMC value determined by the statistical analysis of current−distance traces from different experiments is 4.11 ± 0.48 nS (5.3×10^{-5} G_o) for TNPP (Figure 2). Another anchoring group studied herein is the carboxylic acid group. The binding nature of carboxylic acid is not completely understood. However, at least ionic and coordination binding interactions are possible.[17] For the amine group, binding to the gold electrode is generally believed to be via a weak covalent interaction,[17] or the formation of donor−acceptor bonds with undercoordinated gold atoms.[54] The SMC of carboxylic acid and amine-terminated porphyrins are 2.67 ± 0.26 (3.50×10^{-5} G_o) and 5.91 ± 0.40 nS (7.63×10^{-5} G_o) for TCPP and TAPP, respectively. The SMC value of TAPP is more than twice that of TCPP, which is consistent with reports that amines have a stronger binding to gold than carboxylic acids.[17] Current−distance traces and corresponding current histograms are shown in the Supporting Information and the SMC for all studied molecules are compiled in Figure S1 and Table 1. A direct comparison of the current histograms of these molecules (Figure 6) shows that pyridine-terminated molecules have the highest conductance, and the carboxylic acid terminated species have the smallest SMC value.

Break junction experiments were also carried out, under the same conditions, on 5,10,15,20-tetraphenyl-21*H*,23*H*-porphine

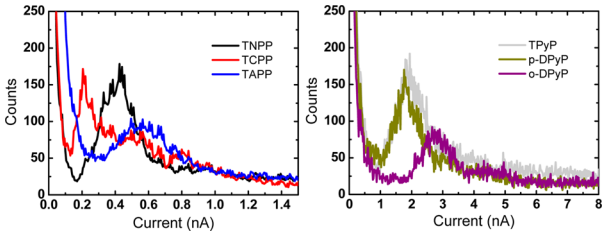

Figure 6. Current histograms constructed from current−distance traces measured at V_{bias} = 0.1 V for tetra(cyano/nitrile)porphine (TNPP, black), tetra(4-carboxyphenyl)porphine (TCPP, red), tetra(4-aminophenyl)porphine (TAPP, blue), tetra(4-pyridyl)porphine (TPyP, gray), 5,15-di(4-pyridyl)-10,20-diphenylporphyrin (p-DPyP, dark yellow), and 5,10-di(4-pyridyl)-15,20-diphenylporphyrin (o-DPyP, magenta), respectively.

(TPP)—a porphyrin having the same porphine core structure but with four phenyl anchoring groups. In principle, it is possible that TPP could form a molecular junction via the phenyl groups by means of the π interaction between an electrode and a phenyl ring.[33,55] From our SMC experiments of TPP, two sets of typical traces were observed: quasi-exponential decay traces (inset, black) and traces (~3% of total curves) having some noise or distortion (Figure 7). For this specific set

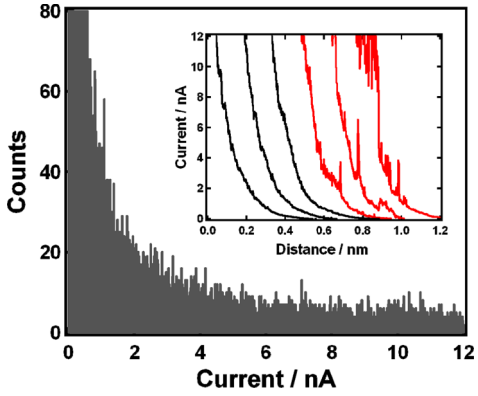

Figure 7. Current histogram and example individual current−distance traces (inset) at a bias of 0.1 V for 5,10,15,20-tetraphenyl-21*H*,23*H*-porphine (TPP). Two sets of typical traces were observed: quasi-exponential decay traces (inset, black) and traces (~3% of total curves) having some noise or distortion. A total of 39 traces with noise or distortion were found from a total of 1376 traces and used to build the current histogram.

of data, 39 traces with noise or distortion were found from a total of 1376 traces and used to build the current histogram which shows no current peak (Figure 7), contrary to the other porphyrins. The current−distance traces detected for THPP are similar to those for TPP and the current histograms show no current peak corresponding to a well-defined molecular conductance precluding the determination of the SMC of porphyrins terminated with hydroxyl (−OH) functional groups. A possible reason could be that the interaction between electrodes and hydroxyl (−OH) groups is too weak to form stable junctions. Hopefully, the present study could stimulate experiments by using other methods or measuring techniques to explore this issue.

SMC data for all porphyrins, compiled in Table 1 and Figure S1, show that the conductance values follow the sequence of o-DPyP > p-DPyP ≈ TPyP > TAPP > TSPP > TNPP > TCPP. This suggests that there is a clear anchoring effect as all the molecules have a common core structure (R2 in Figure 1B).

dx.doi.org/10.1021/jp309871d | J. Phys. Chem. C 2013, 117, 14890−14898

Furthermore, it can be deduced that the anchoring effect follows the sequence of pyridyl > amine ($-NH_2$) > sulfonate ($-SO_3^-$) > nitrile ($-CN$) > carboxylic acid ($-COOH$) in terms of the enhancement of molecular conductance. The observation that pyridyl-terminated porphyrins have the highest conductance may be rationalized by remarking that, in pyridine, the N atoms are directly connected to the aromatic phenyl ring. Thus the electrode contact with pyridyl-terminated porphyrins has the highest conjugation and shortest metal−Molecule−metal (m−M−m) junction distance. On the contrary, molecules with other anchoring groups all have additional bonds between the phenyl ring and the atoms of anchoring groups. The observed high conductance for pyridyl-porphyrins is well-supported by the single molecule study of perylene derivatives (PTCDI) by Tao et al., who found that pyridyl-terminated PTCDI is even more conductive than a phenylthiol terminated PTCDI though thiol is well-known to form strong thiol−gold covalent bonds.[57] As discussed above, the binding strength could be one of the reasons causing the conductance of TAPP to be higher than TCPP. Furthermore, the fact that TCPP has the lowest conductance compared with all other molecules is consistent with density functional theory and nonequilibrium Green's function formalism calculations by Sheng et al. that concluded that in addition to the weaker binding strength, molecules terminated with carboxylic acids have lower conductivity compared to similar molecules with amine anchors because of increased junction length.[58]

It is worth noting that, though it is assumed that the electron donating or withdrawing properties of these anchoring groups should influence the electron density of conjugated porphyrin core structures, it did not dramatically change the HOMO−LUMO gap of these molecules. Our theoretical calculations show that electron donating groups, e.g., $-NH_2$, and $-OH$, can raise the frontier orbital energies compared with TPP. On the contrary, electron-withdrawing groups decrease the LUMO and HOMO of the corresponding molecules. However, these shifts in the energy of the HOMO and LUMO are fairly uniform and the gaps of all the molecules studied here change very little (Table 1). This conclusion is supported by UV−vis data (Figure S4) showing that the side groups only have a negligible effect on the HOMO−LUMO gap of these compact and simple porphyrins. The different anchoring groups only slightly shift (by less than 15 nm) the Soret and Q-band in the UV−vis spectra (Figure S4). For example, the Soret band shifts from 418 to 429 nm when the $-COOH$ groups are replaced by $-NH_2$ side groups (Figure S4). Thus, the difference in conductance for these structurally similar porphyrins appears to arise from factors other than changes in the HOMO−LUMO gap of the molecules.[59]

To better understand the conductance properties of these porphyrin molecules, we also carried out electron transport calculations for the systems containing the various anchoring groups. One example of a transmission spectrum is given in Figure 8 for the TPyP molecule. We see a sharp peak just above the E_F and a large gap of ca. 1.7 eV separating it from the nearest peak below E_F. At first glance, one would assume that these correspond to electron transport through the HOMO and LUMO levels of the molecule. To confirm this assessment, we compare the scattering states associated with these transmission peaks with the MOs of the isolated molecule,[51] as shown in Figure 9. From the symmetry of the porphyrin part in each case, it is clear that indeed the peak at 0.03 eV corresponds to transmission through the LUMO of the isolated

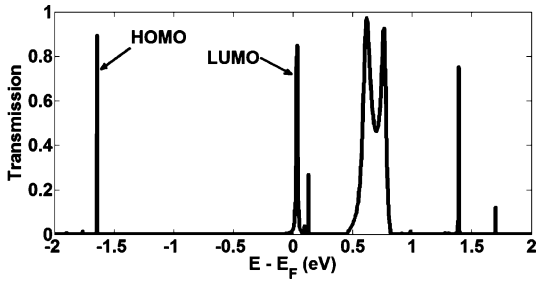

Figure 8. Transmission spectrum for the TPyP molecule. Energy is relative to the Fermi level of the quasi 1-D electrodes shown in Figure 4. The peaks are labeled according to the MOs that contribute to transmission at those energies, as determined from scattering state analysis.

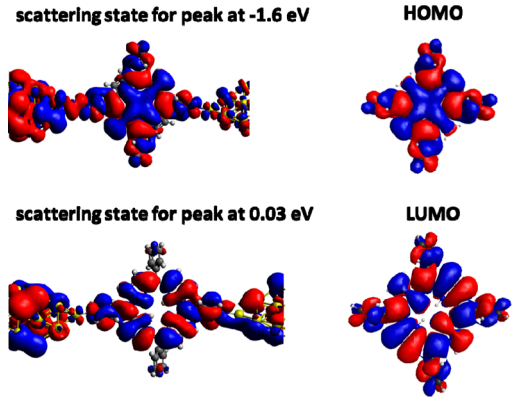

Figure 9. Comparison of scattering states of the two-probe system with MOs of the isolated molecule.

molecule and the peak near −1.6 eV corresponds to transport through the HOMO. Note that the separation between these peaks is smaller than the HOMO−LUMO gap presented in Table 1. This is due to the shifts in energy due to the hybridization of these states with the electrode states.

The transmission spectra for the other molecules are quite similar to the spectrum in Figure 8; there is a sharp peak just above E_F and another peak near −1.6 eV. Scattering state analysis confirms that these correspond to the LUMO and HOMO, respectively, of the isolated molecule, for all molecules considered in this work. The important point is that transmission through the LUMO will dominate in these systems at low bias since it is the nearest molecular level to E_F. It is reasonable that this is consistent for all molecules since the large central porphyrin part of the molecule is the same, and the effect of different anchoring groups is to shift slightly the MO energies and modulate the interaction with the electrodes.

Figure 10 shows a close-up of the LUMO transmission peak for the different molecules studied in this work. The transmission near E_F is related to the low bias SMC. For these systems, this corresponds to the tail of the transmission curve just above E_F. The TPyP and p-DPyP molecules have the highest conductance, and TAPP and TNPP have lower conductance values. However, the o-DPyP has a surprisingly low transmission at E_F. This may be attributed to a binding geometry in the simulation that does not match experiment well. For this molecule, the anchoring groups are closer together (at "ortho" positions) than for the other system, so it is possible that the geometries sampled experimentally are quite different from the simplified one used for the transport

dx.doi.org/10.1021/jp309871d | J. Phys. Chem. C 2013, 117, 14890−14898

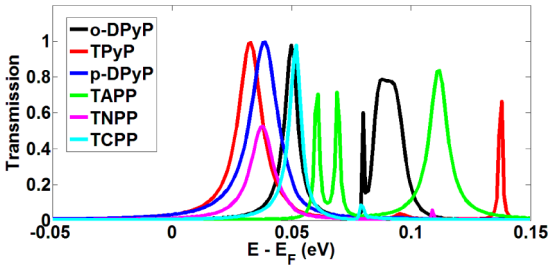

Figure 10. Transmission spectra near E_F for the porphyrins with different anchoring groups.

calculation. In any case, by looking at the heights of the transmission peaks, we can see that the pyridyl groups have overall higher and broader peaks than the systems containing other anchoring groups. This is again due to the strong interaction of pyridyl with the Au electrodes, as determined from the binding energy (see Table 1). Also, note that the pyridyl-containing molecules are the only systems where the anchoring atom is directly part of the π-system of the benzene ring, while for the other systems it is attached to the ring and the single bonds intervene. This direct access to the π-system of the ring may explain the better contact through the pyridyl moiety. While a direct relationship between the SMC and a single parameter from those discussed above is not obvious, it appears that a combination of these factors determines the overall conductance of the molecule. These include the overall length of the molecule, the interaction strength between the anchoring groups and electrodes, and the alignment of the LUMO level with the E_F of the electrodes. There are also other factors which could influence the conductance but were not taken into account in this work. For example, the exact contact geometries of the electrode−molecule junctions could not be known in the experiments and may be different from the ones used for the calculations. In fact, they fluctuate extensively, so that any single geometry computation cannot capture the transport distribution seen in the measurements. This could explain the discrepancy between the experimental and calculation results presented here.

Previous experiments demonstrated that the conductivity of TPyP and p-DPyP was similar and almost 50% lower than the conductivity of o-DPyP.[37] This does not seem to be captured by the calculations, which are about the highest level possible for this size of molecule−electrode junctions. It is clear that the absence of significant agreement between experiments and theory should motivate improvements in both. For instance, experiments should strive for better defined and more reproducible junction geometries, while developments in theoretical methods should both aim to include the effects of solvent and chemisorption induced shifts in E_F, and attempt to reproduce the histograms actually measured by using dynamics computations to select a series of geometries.

CONCLUSION

To summarize, we report a direct comparison of the influence of anchoring groups on electron transport through a series of porphyrins, representing the first attempt to explore the anchoring group effect on single molecule conductance using up to 7 anchoring groups and a single molecular core. Single molecule conductance (SMC) with 2 novel anchoring groups, sulfonate ($-SO_3^-$) and hydroxyl (−OH), were explored, demonstrating that sulfonate represents a new candidate for the reliable construction of molecular junctions. Our results reveal that the single molecule conductance of porphyrins follows the sequence o-DPyP > p-DPyP ≈ TPyP > TAPP > TSPP > TNPP > TCPP (conductance of TPP and THPP is not detectable in our experiments), manifesting a clear anchoring group effect. The demonstration of a general trend of the effect of anchoring groups and the exploration of new anchoring groups reported in this paper may have wider impact in molecule-based devices, functional porphyrin design, and electron transfer/transport studies.

ASSOCIATED CONTENT

Supporting Information

Table of molecular structures and single molecule conductance vs molecular length, individual current−distance traces, corresponding current histograms for different porphyrins, and UV−vis spectra of 9 porphyrins studied. This material is available free of charge via the Internet at http://pubs.acs.org.

AUTHOR INFORMATION

Corresponding Author

* Tel: 847-491-5371 (M.A.R.) and 215-204-9696 (E.B.). Fax: 847-491-7713 (M.A.R.) and 215-204-1532 (E.B.). E-mail: ratner@northwestern.edu (M.A.R.) and eborguet@temple.edu (E.B.).

Notes

The authors declare no competing financial interest.

ACKNOWLEDGMENTS

We thank Lan Nguyen for help with measuring UV−vis of studied porphyrins, and Dr. Yangjun Xing for help with software for analysis of single molecule conductance data. Financial support from the National Science Foundation (CHE 0809838) is gratefully acknowledged. M.S. thanks the FRQNT and the NSF (CHE-1058896) for financial support. M.A.R. thanks the Chemistry Division of the NSF (CHE-1058896) for support.

REFERENCES

(1) Bonifas, A. P.; McCreery, R. L. Assembling Molecular Electronic Junctions One Molecule at a Time. *Nano Lett.* **2011**, *11*, 4725−4729.
(2) Kiguchi, M.; Takahashi, T.; Takahashi, Y.; Yamauchi, Y.; Murase, T.; Fujita, M.; Tada, T.; Watanabe, S. Electron Transport through Single Molecules Comprising Aromatic Stacks Enclosed in Self-Assembled Cages. *Angew. Chem., Int. Ed.* **2011**, *50*, 5707−5710.
(3) Diez-Perez, I.; Li, Z.; Hihath, J.; Li, J. H.; Zhang, C. Y.; Yang, X. M.; Zang, L.; Dai, Y. J.; Feng, X. L.; Muellen, K.; et al. Gate-Controlled Electron Transport in Coronenes as a Bottom-Up Approach towards Graphene Transistors. *Nat. Commun.* **2010**, *1*, 1−5.
(4) Tao, N. J. Electron Transport in Molecular Junctions. *Nat. Nanotechnol.* **2006**, *1*, 173−181.
(5) van der Molen, S. J.; Liljeroth, P. Charge Transport through Molecular Switches. *J. Phys.: Condens. Matter* **2010**, *22*, 133001(1−30).
(6) Nitzan, A.; Ratner, M. A. Electron Transport in Molecular Wire Junctions. *Science* **2003**, *300*, 1384−1389.
(7) Lindsey, J. S.; Bocian, D. F. Molecules for Charge-Based Information Storage. *Acc. Chem. Res.* **2011**, *44*, 638−650.
(8) Chang, S.; He, J.; Zhang, P. M.; Gyarfas, B.; Lindsay, S. Gap Distance and Interactions in a Molecular Tunnel Junction. *J. Am. Chem. Soc.* **2011**, *133*, 14267−14269.
(9) Xu, B. Q.; Tao, N. J. Measurement of Single-Molecule Resistance by Repeated Formation of Molecular Junctions. *Science* **2003**, *301*, 1221−1223.
(10) Kiguchi, M.; Miura, S.; Hara, K.; Sawamura, M.; Murakoshi, K. Conductance of a Single Molecule Anchored by an Isocyanide

Substituent to Gold Electrodes. *Appl. Phys. Lett.* **2006**, *89* (21), 213104(1−3).
(11) Venkataraman, L.; Klare, J. E.; Nuckolls, C.; Hybertsen, M. S.; Steigerwald, M. L. Dependence of Single-Molecule Junction Conductance on Molecular Conformation. *Nature* **2006**, *442*, 904−907.
(12) van Zalinge, H.; Schiffrin, D. J.; Bates, A. D.; Starikov, E. B.; Wenzel, W.; Nichols, R. J. Variable-Temperature Measurements of the Single-Molecule Conductance of Double-Stranded DNA. *Angew. Chem., Int. Ed.* **2006**, *45*, 5499−5502.
(13) Vonlanthen, D.; Mishchenko, A.; Elbing, M.; Neuburger, M.; Wandlowski, T.; Mayor, M. Chemically Controlled Conductivity: Torsion-Angle Dependence in a Single-Molecule Biphenyldithiol Junction. *Angew. Chem., Int. Ed.* **2009**, *48*, 8886−8890.
(14) Xing, Y. J.; Park, T. H.; Venkatramani, R.; Keinan, S.; Beratan, D. N.; Therien, M. J.; Borguet, E. Optimizing Single-Molecule Conductivity of Conjugated Organic Oligomers with Carbodithioate Linkers. *J. Am. Chem. Soc.* **2010**, *132*, 7946−7956.
(15) Arroyo, C. R.; Leary, E.; Castellanos-Gomez, A.; Rubio-Bollinger, G.; Gonzalez, M. T.; Agrait, N. Influence of Binding Groups on Molecular Junction Formation. *J. Am. Chem. Soc.* **2011**, *133*, 14313−14319.
(16) Lortscher, E.; Cho, C. J.; Mayor, M.; Tschudy, M.; Rettner, C.; Riel, H. Influence of the Anchor Group on Charge Transport through Single-Molecule Junctions. *ChemPhysChem* **2011**, *12*, 1677−1682.
(17) Chen, F.; Li, X. L.; Hihath, J.; Huang, Z. F.; Tao, N. J. Effect of Anchoring Groups on Single-Molecule Conductance: Comparative Study of Thiol-, Amine-, and Carboxylic-Acid-Terminated Molecules. *J. Am. Chem. Soc.* **2006**, *128*, 15874−15881.
(18) Kim, B.; Beebe, J. M.; Jun, Y.; Zhu, X. Y.; Frisbie, C. D. Correlation between HOMO Alignment and Contact Resistance in Molecular Junctions: Aromatic Thiols versus Aromatic Isocyanides. *J. Am. Chem. Soc.* **2006**, *128*, 4970−4971.
(19) Dulic, D.; Pump, F.; Campidelli, S.; Lavie, P.; Cuniberti, G.; Filoramo, A. Controlled Stability of Molecular Junctions. *Angew. Chem., Int. Ed.* **2009**, *48*, 8273−8276.
(20) Tivanski, A. V.; He, Y. F.; Borguet, E.; Liu, H. Y.; Walker, G. C.; Waldeck, D. H. Conjugated Thiol Linker for Enhanced Electrical Conduction of Gold-Molecule Contacts. *J. Phys. Chem. B* **2005**, *109*, 5398−5402.
(21) Mishchenko, A.; Zotti, L. A.; Vonlanthen, D.; Burkle, M.; Pauly, F.; Cuevas, J. C.; Mayor, M.; Wandlowski, T. Single-Molecule Junctions Based on Nitrile-Terminated Biphenyls: A Promising New Anchoring Group. *J. Am. Chem. Soc.* **2011**, *133*, 184−187.
(22) Zotti, L. A.; Kirchner, T.; Cuevas, J. C.; Pauly, F.; Huhn, T.; Scheer, E.; Erbe, A. Revealing the Role of Anchoring Groups in the Electrical Conduction Through Single-Molecule Junctions. *Small* **2010**, *6*, 1529−1535.
(23) Hong, W.; Manrique, D. Z.; Garcia, P. M.; Gulcur, M.; Mishchenko, A.; Lambert, C. J.; Bryce, M. R.; Wandlowski, T. Single Molecular Conductance of Tolanes: an Experimental and Theoretical Study on the Junction Evolution in Dependence on the Anchoring Group. *J. Am. Chem. Soc.* **2012**, *134*, 2292−2304.
(24) Tam, E. S.; Parks, J. J.; Shum, W. W.; Zhong, Y. W.; Santiago-Berrios, M. B.; Zheng, X.; Yang, W. T.; Chan, G. K. L.; Abruna, H. D.; Ralph, D. C. Single-Molecule Conductance of Pyridine-Terminated Dithienylethene Switch Molecules. *ACS Nano* **2011**, *5*, 5115−5123.
(25) Martin, C. A.; Ding, D.; Sorensen, J. K.; Bjornholm, T.; van Ruitenbeek, J. M.; van der Zant, H. S. J. Fullerene-Based Anchoring Groups for Molecular Electronics. *J. Am. Chem. Soc.* **2008**, *130*, 13198−13199.
(26) Leary, E.; Gonzalez, M. T.; van der Pol, C.; Bryce, M. R.; Filippone, S.; Martin, N.; Rubio-Bollinger, G.; Agrait, N. Unambiguous One-Molecule Conductance Measurements under Ambient Conditions. *Nano Lett.* **2011**, *11*, 2236−2241.
(27) Boardman, B. M.; Widawsky, J. R.; Park, Y. S.; Schenck, C. L.; Venkataraman, L.; Steigerwald, M. L.; Nuckolls, C. Conductance of Single Cobalt Chalcogenide Cluster Junctions. *J. Am. Chem. Soc.* **2011**, *133*, 8455−8457.
(28) Ko, C. H.; Huang, M. J.; Fu, M. D.; Chen, C. H. Superior Contact for Single-Molecule Conductance: Electronic Coupling of Thiolate and Isothiocyanate on Pt, Pd, and Au. *J. Am. Chem. Soc.* **2010**, *132*, 756−764.
(29) Venkataraman, L.; Klare, J. E.; Tam, I. W.; Nuckolls, C.; Hybertsen, M. S.; Steigerwald, M. L. Single-Molecule Circuits with Well-Defined Molecular Conductance. *Nano Lett.* **2006**, *6*, 458−462.
(30) Chen, W. B.; Widawsky, J. R.; Vazquez, H.; Schneebeli, S. T.; Hybertsen, M. S.; Breslow, R.; Venkataraman, L. Highly Conducting pi-Conjugated Molecular Junctions Covalently Bonded to Gold Electrodes. *J. Am. Chem. Soc.* **2011**, *133*, 17160−17163.
(31) Kiguchi, M.; Takahashi, T.; Kanehara, M.; Teranishi, T.; Murakoshi, K. Effect of End Group Position on the Formation of a Single Porphyrin Molecular Junction. *J. Phys. Chem. C* **2009**, *113*, 9014−9017.
(32) Qian, G. G.; Saha, S.; Lewis, K. M. Two-State Conductance in Single Zn Porphyrin Molecular Junctions. *Appl. Phys. Lett.* **2010**, *96*, 243107(1−3).
(33) Perrin, M. L.; Prins, F.; Martin, C. A.; Shaikh, A. J.; Eelkema, R.; van Esch, J. H.; Briza, T.; Kaplanek, R.; Kral, V.; van Ruitenbeek, J. M.; van der Zant, H. S. J.; Dulic, D. Influence of the Chemical Structure on the Stability and Conductance of Porphyrin Single-Molecule Junctions. *Angew. Chem., Int. Ed.* **2011**, *50*, 11223−11226.
(34) Sedghi, G.; García-Suárez, V. M.; Esdaile, L. J.; Anderson, H. L.; Lambert, C. J.; Martin, S.; Bethell, D.; Higgins, S. J.; Elliott, M.; Bennett, N.; Macdonald, J. E.; Nichols, R. J. Long-Range Electron Tunnelling in Oligo-Porphyrin Molecular Wires. *Nat. Nanotechnol.* **2011**, *6*, 517−522.
(35) Sedghi, G.; Sawada, K.; Esdaile, L. J.; Hoffmann, M.; Anderson, H. L.; Bethell, D.; Haiss, W.; Higgins, S. J.; Nichols, R. J. Single Molecule Conductance of Porphyrin Wires with Ultralow Attenuation. *J. Am. Chem. Soc.* **2008**, *130*, 8582−8583.
(36) Sedghi, G.; Esdaile, L. J.; Anderson, H. L.; Martin, S.; Bethell, D.; Higgins, S. J.; Nichols, R. J. Comparison of the Conductance of Three Types of Porphyrin-Based Molecular Wires: β, meso, β-Fused Tapes, meso-Butadiyne-Linked Twisted meso-meso Linked Oligomers. *Adv. Mater.* **2012**, *24*, 653−657.
(37) Li, Z.; Borguet, E. Determining Charge Transport Pathways through Single Porphyrin Molecules Using Scanning Tunneling Microscopy Break Junctions. *J. Am. Chem. Soc.* **2012**, *134*, 63−66.
(38) Li, Z.; Park, T. H.; Rawson, J.; Therien, M. J.; Borguet, E. Quasi-Ohmic Single Molecule Charge Transport through Highly Conjugated meso-to-meso Ethyne-Bridged Porphyrin Wire. *Nano Lett.* **2012**, *12*, 2722−2727.
(39) Schmidt, M. W.; Baldridge, K. K.; Boatz, J. A.; Elbert, S. T.; Gordon, M. S.; Jensen, J. H.; Koseki, S.; Matsunaga, N.; Nguyen, K. A.; Su, S. J.; Windus, T. L.; Dupuis, M.; Montgomery, J. A. General Atomic and Molecular Electronic-Structure System. *J. Comput. Chem.* **1993**, *14*, 1347−1363.
(40) Becke, A. D. Density-Functional Thermochemistry 3: The Role of Exact Exchange. *J. Chem. Phys.* **1993**, *98*, 5648−5652.
(41) Lee, C. T.; Yang, W. T.; Parr, R. G. Development of the Colle-Salvetti Correlation-Energy Formula into a Functional of the Electron-Density. *Phys. Rev. B* **1988**, *37*, 785−789.
(42) Kresse, G.; Hafner, J. Abinio Molecular-Dynamics for Liquid-Metals. *Phys. Rev. B* **1993**, *47*, 558−561.
(43) Kresse, G.; Furthmuller, J. Efficient Iterative Schemes for Ab Initio Total-Energy Calculations Using a Plane-Wave Basis Set. *Phys. Rev. B* **1996**, *54*, 11169−11186.
(44) Perdew, J. P.; Burke, K.; Ernzerhof, M. Generalized Gradient Approximation Made Simple. *Phys. Rev. Lett.* **1996**, *77*, 3865−3868.
(45) Blochl, P. E. Projector Augmented-Wave Method. *Phys. Rev. B* **1994**, *50*, 17953−17979.
(46) Kresse, G.; Joubert, D. From Ultrasoft Pseudopotentials to the Projector Augmented-Wave Method. *Phys. Rev. B* **1999**, *59*, 1758−1775.
(47) http://www.nanoacademic.ca.

(48) Taylor, J.; Guo, H.; Wang, J. Ab Initio Modeling of Quantum Transport Properties of Molecular Electronic Devices. *Phys. Rev. B* **2001**, *63*, 245407(1−13).
(49) Waldron, D.; Haney, P.; Larade, B.; MacDonald, A.; Guo, H. Nonlinear Spin Current and Magnetoresistance of Molecular Tunnel Junctions. *Phys. Rev. Lett.* **2006**, *96*, 166804(1−4).
(50) Sancho, M. P. L.; Sancho, J. M. L.; Rubio, J. Quick Iterative Scheme for the Calculation of Transfer-Matrices − Application to Mo(100). *J. Phys. F: Met. Phys.* **1984**, *14*, 1205−1215.
(51) One or more scattering states can be attributed to any transmission peak, which can then be projected onto the MOs of the molecule to determine which ones contribute to transmission at a particular energy. Each transmission peak is assigned to the MO that contributes the largest amount to its scattering states. Details on scattering states can be found in ref 48.
(52) Troullier, N.; Martins, J. L. Efficient Pseudopotentials for Plane-Wave Calculations. *Phys. Rev. B* **1991**, *43*, 1993−2006.
(53) Li, X. L.; He, J.; Hihath, J.; Xu, B. Q.; Lindsay, S. M.; Tao, N. J. Conductance of Single Alkanedithiols: Conduction Mechanism and Effect of Molecule-Electrode Contacts. *J. Am. Chem. Soc.* **2006**, *128*, 2135−2141.
(54) Kamenetska, M.; Quek, S. Y.; Whalley, A. C.; Steigerwald, M. L.; Choi, H. J.; Louie, S. G.; Nuckolls, C.; Hybertsen, M. S.; Neaton, J. B.; Venkataraman, L. Conductance and Geometry of Pyridine-Linked Single-Molecule Junctions. *J. Am. Chem. Soc.* **2010**, *132*, 6817−6821.
(55) Solomon, G. C.; Herrmann, C.; Vura-Weis, J.; Wasielewski, M. R.; Ratner, M. A. The Chameleonic Nature of Electron Transport through pi-Stacked Systems. *J. Am. Chem. Soc.* **2011**, *132*, 7887−7889.
(56) The TSPP molecule is omitted because charged molecules in solution cannot be properly treated with the current NEGF-DFT approach used.
(57) Li, X. L.; Hihath, J.; Chen, F.; Masuda, T.; Zang, L.; Tao, N. J. Thermally Activated Electron Transport in Single Redox Molecules. *J. Am. Chem. Soc.* **2007**, *129*, 11535−11542.
(58) Sheng, W.; Li, Z. Y.; Ning, Z. Y.; Zhang, Z. H.; Yang, Z. Q.; Guo, H. Quantum Transport in Alkane Molecular Wires: Effects of Binding Modes and Anchoring Groups. *J. Chem. Phys.* **2009**, *131*, 244712(1−9).
(59) Yoon, H. J.; Shapiro, N. D.; Park, K. M.; Thuo, M. M.; Soh, S.; Whitesides, G. M. The Rate of Charge Tunneling through Self-Assembled Monolayers Is Insensitive to Many Functional Group Substitutions. *Angew. Chem., Int. Ed.* **2012**, *51*, 4658−4661.